

# Multifrequency multisatellite carrier tracking

Kaspar Giger<sup>1</sup>, Patrick Henkel<sup>2</sup>, Christoph Günther<sup>3</sup>

Technische Universität München

Munich, Germany

Email: <sup>1</sup>kaspar.giger@tum.de, <sup>2</sup>patrick.henkel@tum.de

<sup>3</sup>christoph.guenther@tum.de

## BIOGRAPHIES

Kaspar Giger received the M.S. degree in electrical engineering and information technology from the Swiss Federal Institute of Technology (ETH), Zurich, Switzerland, in 2006. In his M.S. thesis, he worked on an implementation and optimization of a real-time MPEG4/AVC H.264 encoder on a TI DM642 DSP platform. He is currently pursuing the Ph.D. degree at the Institute of Communications and Navigation, Technische Universität München, Munich, Germany, working on new carrier tracking algorithms.

Patrick Henkel studied electrical engineering and information technology at the Technische Universität München, Munich, Germany, and the Ecole Polytechnique de Montreal, Montreal, QC, Canada. He is currently pursuing the Ph.D. degree at the Institute of Communications and Navigation, TUM, and his focus is on robust ambiguity resolution for precise carrier-phase positioning with multiple frequencies.

In 2007, he was a Guest Researcher at TU Delft, in 2008 at the GPS Lab at Stanford University, Stanford, CA. Mr. Henkel received the Pierre Contensou Gold Medal at the International Astronautical Congress in 2007.

Christoph Günther studied theoretical physics at the Swiss Federal Institute of Technology (ETH), Zurich, Switzerland. He received his diploma in 1979 and completed his PhD in 1984. He worked on communication and information theory at Brown Boveri and Ascom Tech. From 1995, he led the development of mobile phones for GSM and later dual mode GSM/Satellite phones at Ascom. In 1999, he became head of the research department of Ericsson in Nuremberg. Since 2003, he is the director of the Institute of Communication and Navigation at the German Aerospace Center (DLR) and since December 2004, he additionally holds a Chair at the Technische Universität München, Munich, Germany. His research interests are in satellite navigation, communication, and signal processing.

## ABSTRACT

Carrier-phase measurements on at least two frequencies are required for precise and reliable positioning. Clearly,

the corresponding code- and carrier-phases must be measured with a high precision and reliability. Today's GNSS receivers use individual Phase- and Delay Locked Loops (PLL/DLL) for each tracked satellite on each frequency to measure the phases. Strong atmospheric effects (e.g. ionospheric scintillations), receiver movements (e.g. banking of an aircraft) or RF-interference and jamming can lead to a substantial reduction of the carrier-to-noise ratios of some of the GNSS signals. Although the mentioned effects are usually of limited duration, traditional tracking loops likely loose lock of some of the signals (not all satellites at the same time though). The following re-acquisition is time-consuming and results in a changed carrier-phase ambiguity.

Vector Delay Locked Loops have shown to improve the performance of the code-phase tracking by using the spatial correlation of the received signals. In this paper, the concept is further extended to the more critical carrier-phase tracking. The reliability of the tracking is further enhanced by using the spectral correlation of all the received signals from one satellite which is especially useful for Galileo with three open frequencies.

We show that compared to traditional receivers, the joint tracking receiver needs no re-acquisition and can therefore demodulate a masked signal as soon as it appears again. For short interruptions even cycle slips can be avoided. The noise performance is also compared to the individual tracking approach. We conclude therefore that the Multifrequency Multisatellite Tracking Loop makes carrier-phase tracking more robust in GNSS receivers

## 1. INTRODUCTION

Every received signal is affected by the same receiver movements, by the same receiver clock biases and so forth (more precisely by the projection onto the line-of-sight). Independent tracking loops employed for all signals, as typically used in today's GNSS receivers, neglect their strong spatial and spectral correlation.

Sennott and Senffner were among the first to make use of the spatial correlation of the signals in the phase tracking, [1]. Spilker developed a similar idea for the code tracking loop in the Vector DLL [2]. The idea of vector tracking recently gained interest together with the first Software defined GNSS receivers, e.g. [3]. Henkel et al.

proposed to further exploit the spectral signal correlations [4].

In this paper the concept is further extended by using a dedicated model for all components affecting the received signal. It is shown how the carrier-phase and code-phase tracking can be conducted jointly for all active signals, i.e. for all satellites and all frequencies.

This paper is divided into five sections. After this short introduction follows a detailed description of the carrier-phase tracking problem. All processes affecting the instantaneous carrier-phases of the received signals are explained with their projection onto the signals. The algorithm developed with this detailed model is analyzed in the third section. The evaluation model is first presented and later used to derive the algorithm's performance. The joint tracking is further extended to the code tracking in the fourth section. In the last section, this paper is finally concluded.

## 2. SYSTEM MODEL

Since the early times of implementing phase locked loops digitally, they have been modeled in a state-space framework to allow the usage of Kalman filters, e.g. [5]. The same approach was also used by Hurd et al. to model the phase tracking in GPS receivers [6]. With the advent of software-defined GNSS receivers, this approach to phase tracking has recently gained high attention, cf. [7].

If the phase locked loop is replaced by a Kalman filter, there's no direct hint on how to steer the local oscillator—although this relationship could be derived by using Patapoutian's loop representation<sup>1</sup> [8]. But to have better control of the phase and frequency of the local oscillator, the loop needs to be represented as a control problem [9]. This procedure can be further extended to include the signals from multiple satellites, received at multiple frequencies.

In this section the model used to derive the Multisatellite Multifrequency phase tracking task is detailed.

### PHASE MODEL

The phase of the received signal is first broken down into the parts originating from the receiver motion, the receiver oscillator, the atmosphere and the satellite's oscillator [10]:

$$\begin{aligned}\varphi_m^k(t) &= \phi_m^k(t - \tau_m^k(t)) \\ &= \phi_{0,m}^k + 2\pi f_{c,m}^k(t - \tau_m^k(t)) \\ &= \phi_m^k(t) + 2\pi f_{c,m}^k \tau_m^k(t),\end{aligned}$$

with

$$\begin{aligned}\tau_m^k(t) &= \frac{1}{c} \left( (\mathbf{e}^k)^T [\mathbf{r}(t) - \mathbf{r}^k(t')] + c\delta(t) \right. \\ &\quad \left. + c\delta^k(t') - I_m^k(t'') + T^k(t''') \right).\end{aligned}$$

<sup>1</sup>With  $\hat{\mathbf{x}}_k$  denoting the estimated phase and its derivatives:  $\omega_{\text{NCO},i+1} = \frac{1}{T} \mathbf{C} \mathbf{A} (\hat{\mathbf{x}}_{i+1} - \hat{\mathbf{x}}_i)$ .

The following denotations are used:

$m$	the carrier frequency ( $1 \dots M$ ),
$k$	the satellite ( $1 \dots K$ ),
$\mathbf{e}^k$	unit vector pointing from the $k$ -th satellite to the receiver,
$\mathbf{r}, \mathbf{r}^k$	the locations of the receiver and satellite $k$ in the same Cartesian coordinate system (e.g. ECEF),
$\delta, \delta^k$	the receiver and satellite clock bias (in seconds),
$I_m^k$	the ionospheric delay (in meters),
$T^k$	the tropospheric delay (in meters),
$t'$	the time when the signal (received at time $t$ ) was emitted,
$t''$	the time when the signal hit the ionosphere (simplifying the ionosphere as a thin shell) and
$t'''$	the time when the signal hit the ionosphere (same simplification).

Each part is modeled as a random walk, driven by white Gaussian noise [11]. Denoting by  $n_x$  the order of the derivative represented by the noise sequence, Taylor's theorem can be used to characterize the evolution over time of the process  $x(t)$ :<sup>2</sup>

$$x(t+T) = \sum_{l=0}^{n_x-1} x^{(l)}(t) \frac{T^l}{l!} + R_{x,n_x}(t+T, t, n_x), \quad (1)$$

defining the general remainder term as

$$R_{x,n_x}(t_2, t_1, l) = \int_{t_1}^{t_2} w_x(u) \frac{(t_2 - u)^{n_x - l - 1}}{(n_x - l - 1)!} du.$$

The same expansion can clearly be carried out for higher derivatives of  $x(t)$ . Using the above definition, the derivatives of the random processes can be stacked into a vector, resulting in

$$\underbrace{\begin{bmatrix} x^{(0)}(t_{i+1}) \\ \vdots \\ x^{(n_x-1)}(t_{i+1}) \end{bmatrix}}_{\mathbf{x}_x(t_{i+1})} = \mathbf{A}_{n_x} \mathbf{x}_x(t_i) + \underbrace{\begin{bmatrix} R_{x,n_x}(t_{i+1}, t_i, n_x) \\ \vdots \\ R_{x,n_x}(t_{i+1}, t_i, 1) \end{bmatrix}}_{\mathbf{w}_{x,i+1}},$$

with  $(\mathbf{A}_{n_x})_{h,j} = \begin{cases} \frac{T^{j-h}}{(j-h)!}, & \text{if } j-h \geq 0 \\ 0 & \text{otherwise} \end{cases}$   
and  $T = t_{i+1} - t_i$

Plugging in the expansions for the above mentioned parts influencing the signal phase, a state-space model for the

<sup>2</sup>Although the Taylor's theorem assumes sufficiently smooth functions, which is not true for a white noise sequence

received signal phase emerges

$$\begin{aligned}
\varphi_{m,i+1}^k &= \mathbf{x}_{\phi,i+1} + (\mathbf{e}^k)^T \otimes \mathbf{I}_{n_r} (\mathbf{x}_{r,i+1} - \mathbf{x}_{r^k,i+1}) \\
&\quad + \mathbf{x}_{\delta,i+1} + \mathbf{x}_{\delta^k,i+1} + \mathbf{x}_{I_m^k,i+1} + \mathbf{x}_{T^k,i+1} \\
&= \mathbf{A}_n \left( \mathbf{x}_{\phi,i} + (\mathbf{e}^k)^T (\mathbf{x}_{r,i} - \mathbf{x}_{r^k,i}) + \mathbf{x}_{\delta,i} \right. \\
&\quad \left. + \mathbf{x}_{\delta^k,i} + \mathbf{x}_{I_m^k,i} + \mathbf{x}_{T^k,i} \right) \\
&\quad + \frac{2\pi}{\lambda_m} \left( (\mathbf{e}^k)^T \otimes \mathbf{I}_{n_r} (\mathbf{w}_{r,i+1} - \mathbf{w}_{r^k,i+1}) \right. \\
&\quad \left. + \mathbf{w}_{\delta,i+1} + \mathbf{w}_{\delta^k,i+1} + \mathbf{w}_{I_m^k,i+1} + \mathbf{w}_{T^k,i+1} \right) \quad (2)
\end{aligned}$$

having  $n = \max(n_\phi, n_r, n_{r^k}, n_\delta, n_{\delta^k}, n_I, n_T)$ .

Not all of the processes have the order  $n$ . The state-vector of those with reduced order are augmented by a sufficient number of zero-valued entries.

## NCO MODEL

In analogy to the beforehand derived model for the received signal phase (and its derivatives), a model for the Numerically Controlled Oscillator has to be found. In contrast to the phase-model, the states of the NCO are driven by a user-defined input signal rather than (process) noise.

The unsteered NCO (zero input) just generates a sinusoidal signal at a certain frequency, having a continuous phase:

$$\begin{aligned}
\omega_{\text{NCO},i+1} &= \omega_{\text{NCO},i} \\
\varphi_{\text{NCO},i+1} &= \varphi_{\text{NCO},i} + T\omega_{\text{NCO},i}.
\end{aligned}$$

Allowing the frequency and the phase to be changed between successive intervals, the following NCO model arises<sup>3</sup>:

$$\underbrace{\begin{bmatrix} \varphi_{\text{NCO},m,i+1}^k \\ \omega_{\text{NCO},m,i+1}^k \\ 0 \\ \vdots \end{bmatrix}}_{\varphi_{\text{NCO},m,i+1}^k} = \mathbf{A}_n \varphi_{\text{NCO},m,i}^k + \underbrace{\begin{bmatrix} \mathbf{I}_2 \\ \mathbf{0} \\ -\mathbf{B}_0 \end{bmatrix}}_{-\mathbf{B}_0} \mathbf{u}_{\varphi,m,i}^k \quad (3)$$

## PLANT MODEL

Having in mind the outcome of the correlation integral of two sinusoidal signals, the difference of Equations 2 and 3 can be used, like described in [12], to finally describe the plant of the phase control system (for one individual

<sup>3</sup>The state-vector could as well be augmented by higher order derivatives of the NCO-phase, leading to a higher order NCO. However in this text only second-order NCOs are considered.

signal):

$$\underbrace{(\varphi_{m,i+1}^k - \varphi_{\text{NCO},m,i+1}^k)}_{\mathbf{x}_{\varphi,m,i+1}^k} = \mathbf{A}_n \mathbf{x}_{\varphi,m,i}^k + \frac{2\pi}{\lambda_m} \left( (\mathbf{e}^k)^T \otimes \mathbf{I}_{n_r} \cdot (\mathbf{w}_{r,i+1} - \mathbf{w}_{r^k,i+1}) + \mathbf{w}_{\delta,i+1} + \mathbf{w}_{\delta^k,i+1} + \mathbf{w}_{I_m^k,i+1} + \mathbf{w}_{T^k,i+1} \right) + \mathbf{B}_0 \mathbf{u}_{\varphi,m,i}^k \quad (6)$$

Taking a closer look at the noise terms (or remainder terms of the Taylor expansion), the contributions from several satellites/frequencies are correlated or simply scaled.

**Receiver movements** Assuming uncorrelated movements in the three spatial dimensions, their projection onto the line-of-sight vector is observed in the phase-domain:

$$\varphi_{r_m}^k(t) = \frac{2\pi}{\lambda_m} \left( (\mathbf{e}^k)^T \mathbf{r}(t) \right)$$

The Taylor expansion like performed in Equation 1 is in theory not valid, since the unit vector  $\mathbf{e}^k$  might be changing during the interval of consideration. The expected rate of change is in the order of less than  $10^{-3}$  per second and therefore neglected in this analysis. Hence the noise terms are scaled by the unit vectors at the beginning of the interval.

**Satellite movements** The movements of the satellites are given with a high and sufficient precision (e.g. Broadcast or IGS ephemerides). Due to their smooth dynamics the satellites can be modeled as having a constant acceleration over the interval of consideration. The remainder terms of the Taylor series are then simplified as

$$\mathbf{w}_{r^k,i+1} = \left[ R_{r_x^k,2}(t_{i+1}, t_i, 2), R_{r_x^k,2}(t_{i+1}, t_i, 1), 0, \dots, R_{r_y^k,2}(t_{i+1}, t_i, 2), \dots \right]^T$$

with

$$\begin{aligned}
R_{r_x^k,2}(t_{i+1}, t_i, l) &= \int_{t_i}^{t_{i+1}} \ddot{r}_x^k(u) (t_{i+1} - u)^{l-1} du \\
&\approx \ddot{r}_x^k(t_i) \frac{T^l}{l}, \quad l \in \{1, 2\}
\end{aligned}$$

The impact of the satellite movements is therefore deterministic and can be seen as reference input to the phase-system. As we want to follow the phase of the received signal, the same input has to be used for the local system, i.e. the NCO:

$$\mathbf{u}_{\text{ref},m,i}^k = \frac{2\pi}{\lambda_m} (\mathbf{e}^k)^T \ddot{\mathbf{r}}_i^k \begin{bmatrix} T^2/2 \\ T \end{bmatrix}.$$

**Ionospheric delay** For any satellite, the ionospheric delay is proportional with the carrier frequency<sup>4</sup>. Therefore

<sup>4</sup>Simplifying the ionospheric delays to their first order effect.

$$\mathbf{G}_\varphi = 2\pi \cdot \begin{bmatrix} \boldsymbol{\mu} \otimes (\mathbf{e}^1)^T & \boldsymbol{\mu} & \boldsymbol{\mu} & \mathbf{0} & \dots & \mathbf{q} \cdot \boldsymbol{\mu} & \mathbf{0} & \dots & m^1 \boldsymbol{\mu} & \mathbf{0} & \dots \\ \boldsymbol{\mu} \otimes (\mathbf{e}^2)^T & \boldsymbol{\mu} & \mathbf{0} & \boldsymbol{\mu} & \dots & \mathbf{0} & \mathbf{q} \cdot \boldsymbol{\mu} & \dots & \mathbf{0} & m^2 \boldsymbol{\mu} & \dots \\ \vdots & \vdots & \vdots & \vdots & \ddots & \vdots & \vdots & \ddots & \vdots & \vdots & \ddots \end{bmatrix} \otimes \mathbf{I}_n \quad (4)$$

$$= 2\pi \cdot [\mathbf{H} \otimes \boldsymbol{\mu}, \mathbf{I}_K \otimes \boldsymbol{\mu}, \mathbf{I}_K \otimes (\mathbf{q} \cdot \boldsymbol{\mu}), \text{diag}(m^1, \dots, m^K) \otimes \boldsymbol{\mu}] \otimes \mathbf{I}_n \quad (5)$$

the remainder terms in Equation 6 are scaled by their frequency-factor  $q$ :

$$\text{with } I_m^k(t) = q_m^2 I_0^k(t), \text{ and } q_m = \frac{f_0}{f_m} :$$

$$(\mathbf{w}_{I_m^k, i+1})_l = \begin{cases} q_m^2 R_{I_0^k, n_I}(t_{i+1}, t_i, n_I - l + 1), & \text{for } l = 1, \dots, n_I \\ 0 & \text{otherwise} \end{cases}$$

**Tropospheric delay** The tropospheric delay encountered by the signals received from a satellite can be separated in their dry- and wet-component and their respective mapping function<sup>5</sup> [10]:

$$T^k(t) = m^k(t) \underbrace{(T_{Z, \text{dry}}(t) + T_{Z, \text{wet}}(t))}_{T_Z(t)}$$

Like in the preceding paragraphs the Taylor expansion is also performed for the tropospheric zenith delay, assuming that the mapping function is constant during the considered interval.

The plant model can now be summarized by

$$\mathbf{x}_{\varphi, i+1} = \mathbf{A} \mathbf{x}_{\varphi, i} + \mathbf{B} \mathbf{u}_{\varphi, i} + \mathbf{G}_\varphi \mathbf{w}_{i+1},$$

with

$$\mathbf{A} = \mathbf{I}_{K \cdot M} \otimes \mathbf{A}_n,$$

$$\mathbf{B} = \mathbf{I}_{K \cdot M} \otimes \mathbf{B}_0,$$

$$\mathbf{w}_{i+1} = [\mathbf{w}_{r, i+1}^T, \mathbf{w}_{\delta^1, i+1}^T, \mathbf{w}_{\delta^2, i+1}^T, \mathbf{w}_{T_Z}^T, \dots, \mathbf{w}_{I_0^1}, \mathbf{w}_{I_0^2}, \dots, \mathbf{w}_{T_Z}]^T,$$

$$\boldsymbol{\mu} = \left[ \frac{1}{\lambda_1}, \dots, \frac{1}{\lambda_M} \right]^T,$$

$$\mathbf{q} = \text{diag}[q_1^2, \dots, q_M^2]^T,$$

and the matrix  $\mathbf{G}_\varphi$  as defined in Equation 4. Additionally the covariance of the process noise vector  $\mathbf{w}_{i+1}$  has to be defined. By following the approach described above, the covariance matrix can be found in a way, similar to [13]:

$$\mathbb{E}\{\mathbf{w}_i \mathbf{w}_j\} = \delta(i - j) \cdot \mathbf{Q}.$$

The states as defined above are clearly not directly observable and need therefore be estimated by an observer (typically implemented as a Kalman filter). The outcome of the phase-discriminator can be used as the measurements.

<sup>5</sup>Simplified here by a general mapping function.

Following [2], the Inphase- and Quadrature-components are approximated by

$$I_i \approx D_i R(\Delta\tau_i) \cdot \text{sinc}\left(\frac{T}{2} \cdot \overline{\Delta\omega_i}\right) \cdot \cos(\overline{\Delta\varphi_i}) + n_{I, i}$$

$$Q_i \approx D_i R(\Delta\tau_i) \cdot \text{sinc}\left(\frac{T}{2} \cdot \overline{\Delta\omega_i}\right) \cdot \sin(\overline{\Delta\varphi_i}) + n_{Q, i},$$

where  $\overline{\Delta\varphi_i}$  and  $\overline{\Delta\omega_i}$  denote the average phase and frequency offset respectively (over the interval  $[t_{i-1}, t_i]$ ),  $R(\cdot)$  the autocorrelation function of the spreading code,  $\Delta\tau_i$  its offset (w.r.t. the local copy),  $D_i$  the navigation bit and  $n_{I, i}$ ,  $n_{Q, i}$  uncorrelated noise samples. Taking the arctangent of the quotient, leaves just the average phase offset:

$$D_{\varphi, i} = \text{atan}\left(\frac{Q_i}{I_i}\right) \approx \overline{\Delta\varphi_i} + n_{\varphi, i}.$$

This leads to the well-known observation matrix  $\mathbf{C}_n$ , with  $(\mathbf{C}_n)_{1, j} = T^{j-1}/j!$ ,  $j = 1, \dots, n$  (e.g. [7]). In the case of multisatellite and multifrequency tracking a set of measurements is used to estimate the states:

$$[D_{\varphi, m=1, i}^{k=1}, D_{\varphi, 2, i}^1, \dots, D_{\varphi, 1, i}^2, \dots]^T = \underbrace{(\mathbf{I}_{M \cdot K} \otimes \mathbf{C}_n)}_{\mathbf{C}} \mathbf{x}_{\varphi, i} + \mathbf{n}_{\varphi, i}. \quad (7)$$

The covariance matrix of the measurement noise terms  $\mathbf{n}_{\varphi, i}$  is chosen to be diagonal with the entries<sup>6</sup>

$$\left(\mathbb{E}\{\mathbf{n}_{\varphi, i} \mathbf{n}_{\varphi, j}\}\right)_{l, l} = \delta(i - j) \cdot (\mathbf{R})_{l, l} = \frac{\delta(i - j)}{2C_l/N_0 T},$$

where  $C_l/N_0$  is the carrier-to-noise density ratio of the  $l$ -th channel.

## OBSERVABILITY/CONTROLLABILITY

To successfully implement a controller for the plant describe in section , controllability and observability have to be fulfilled.

It can be shown that the observability matrix  $\mathbf{Q}_o$  has rank  $K \cdot M \cdot n$ . Therefore observability after Kalman is fulfilled.

If  $n$  is larger than 2, the condition for controllability after Kalman can not be met. This can be seen from Equation 3, where matrix  $\mathbf{B}_0$  shows empty rows. To solve this problem, either a higher order NCO could be used (not discussed here) or the higher order state-components

<sup>6</sup>In [9], [12] the entries of the covariance matrix are additionally multiplied by  $\left(1 + \frac{1}{2C_l/N_0 T}\right)$ . In [14] it's shown that with a nonlinear interpretation of the measurement noise this additional factor can be neglected.

are treated as a disturbance. In this case the disturbance is estimated by the observer and fed forward on the controller<sup>7</sup>.

### CONTROLLER DESIGN

Finally the feedback law of the controller takes the usual form of a linear controller:

$$\mathbf{u}_{\varphi,i} = -\mathbf{K}\hat{\mathbf{x}}_{\varphi,i}.$$

The poles of the controller can be chosen directly by parametric state feedback design or by using results of optimal control, where the intent is to find the input  $\mathbf{u}$  that minimizes a quadratic cost functional, like described in [9], [12].

### MULTICONSTELLATION TRACKING

From Equation 6 it can be further seen that the multisatellite tracking allows the joint use of different GNSS systems in the tracking (e.g. Galileo and GPS). Assuming that the offsets between the timescales of all used systems are many times more stable than the clock offset of the receiver, the change of it with respect to the system times remains the same for all systems. And after the initial acquisition only relative changes have an influence. Optionally the intersystem clock bias could be included as a further random process, but just having a small variance.

### 3. PERFORMANCE EVALUATION

In this section the performance of the presented multi-frequency and multisatellite is evaluated, first analytically and later by simulation. A linearized and simplified baseband model of the loop is shown in Figure 1. First the transfer functions of the observer (including the feedback path) and the actuator (NCO) are defined, leading then to an overall transfer function.

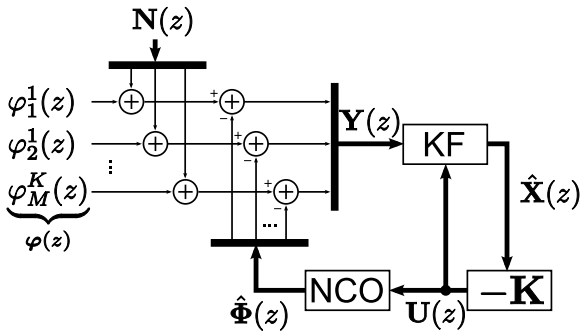


Fig. 1. Simplified baseband model of the multifrequency multisatellite tracking loop (the bold lines represent vector quantities and the bars multi- and demultiplexing operations).

### TRANSFER FUNCTION DERIVATION

<sup>7</sup>If the higher order terms are ignored but treated as disturbance, a constant offset in the phase-discriminator results.

Denoting the Kalman gain by  $\mathbf{L}_i$  the estimated state relates to the discriminator outputs ( $\mathbf{y}_i$ ) by

$$\hat{\mathbf{X}}(z) = (z\mathbf{I} - \mathbf{A} + \mathbf{B} + \mathbf{LCA} - \mathbf{LCBK})^{-1} \mathbf{LY}(z),$$

hence

$$\mathbf{U}(z) = -\mathbf{K}\hat{\mathbf{X}}(z) = \mathbf{H}_o(z)\mathbf{Y}(z) \quad (8)$$

$$\mathbf{H}_o(z) = -\mathbf{K}(z\mathbf{I} - \mathbf{A} + \mathbf{BK} + \mathbf{LCA} - \mathbf{LCBK})^{-1} \mathbf{L}.$$

The NCO output  $\hat{\Phi}(z)$  contains the estimated phase and frequency for each signal. Its relation to the control input  $\mathbf{u}$  can be summarized by the transfer function

$$\begin{aligned} \mathbf{H}_{\text{NCO}}(z) &= (z\mathbf{I} - \mathbf{I}_{K \cdot M} \otimes \mathbf{A}_2)^{-1}, \\ \hat{\Phi}(z) &= \mathbf{H}_{\text{NCO}}(z)\mathbf{U}(z). \end{aligned} \quad (9)$$

The estimated phase is formed by multiplying the vector  $\hat{\Phi}$  with the above defined measurement matrix  $\mathbf{C}$ :

$$\hat{\varphi}(z) = \underbrace{(\mathbf{I}_{K \cdot M} \otimes \mathbf{C}_2)}_{\mathbf{C}_p} \hat{\Phi}(z). \quad (10)$$

And though finally the measurements  $\mathbf{y}$  can be related to the input and the feedback path:

$$\begin{aligned} \mathbf{Y}(z) &= \varphi(z) - \mathbf{C}_p \hat{\Phi}(z) + \mathbf{N}(z), \\ &= (\mathbf{I} + \mathbf{C}_p \mathbf{H}_{\text{NCO}}(z) \mathbf{H}_o(z))^{-1} (\varphi(z) + \mathbf{N}(z)). \end{aligned} \quad (11)$$

Solving for the carrier-phase error  $\Delta = \varphi - \hat{\varphi}$  by using the Equations 8,9,10 and 11 the transfer function of the tracking loop can be found:

$$\begin{aligned} \Delta(z) &= \underbrace{(\mathbf{I} + \mathbf{C}_p \mathbf{H}_{\text{NCO}}(z) \mathbf{H}_o(z))^{-1}}_{\mathbf{H}(z)} \varphi(z) \\ &+ \underbrace{\mathbf{C}_p \mathbf{H}_{\text{NCO}}(z) \mathbf{H}_o(z) (\mathbf{I} + \mathbf{C}_p \mathbf{H}_{\text{NCO}}(z) \mathbf{H}_o(z))^{-1}}_{\mathbf{H}_n(z)} \mathbf{N}(z) \end{aligned} \quad (12)$$

The (measurement) noise sequence  $\mathbf{n}_i$  is assumed to be zero-mean, white and described by its autocovariance function, defining also the spectral density<sup>8</sup>:

$$\begin{aligned} R_n(i, j) &= \delta(i - j) \cdot \mathbb{E} \{ \mathbf{n}_i \mathbf{n}_j^H \}, \\ S_N(z) &= \mathbb{E} \{ \mathbf{n}_i \mathbf{n}_i^H \} = \mathbf{R}, \end{aligned}$$

where  $(\cdot)^H$  denotes the Hermitian transpose.

The covariance of the samples of a zero-mean discrete-time random process  $\nu(i)$  can be computed by the integral over one period of its spectral density [15]:

$$\mathbb{E} \{ \nu_i \nu_j^H \} = \frac{1}{2\pi} \int_{-\pi}^{\pi} S_\nu(e^{j\omega}) d\omega.$$

Plugging in the beforehand derived noise response, results in the carrier-phase error covariance matrix. Unlike in textbooks the quantity derived here is a covariance matrix

<sup>8</sup>The measurement noise covariance matrix used in the Kalman filter (denoted above by  $\mathbf{R}$ ) must not necessarily be equal to the actual covariance of the incoming signal. To distinguish, a tilde is used for the input signal's covariance.

instead of being just a scalar variance value, since the phases of several signals are tracked jointly:

$$\begin{aligned} \text{Cov}(\Delta_n) &= \frac{1}{2\pi} \int_{-\pi}^{\pi} \mathbf{H}_n(e^{j\omega}) \mathbb{E}\{\mathbf{n}_r \mathbf{n}_r^H\} \mathbf{H}_n^H(e^{j\omega}) d\omega \\ &= \frac{1}{2\pi} \int_{-\pi}^{\pi} \mathbf{H}_n(e^{j\omega}) \tilde{\mathbf{R}} \mathbf{H}_n^H(e^{j\omega}) d\omega \quad (13) \end{aligned}$$

In [16] it's shown that the standard deviation of the carrier-phase error marks a good measure for the mean time to cycle slipping in a PLL. Meaning that the lower standard deviation the higher the robustness of the loop.

## NUMERICAL STUDIES

The above derivation can as well be used for the assessment of the phase tracking performance of a one-signal standalone Kalman filter based tracking algorithm. Two examples are compared with IF-simulated (intermediate frequency) signals (see Figure 2). The plots show a good agreement between the analytically derived performance and the simulated one.

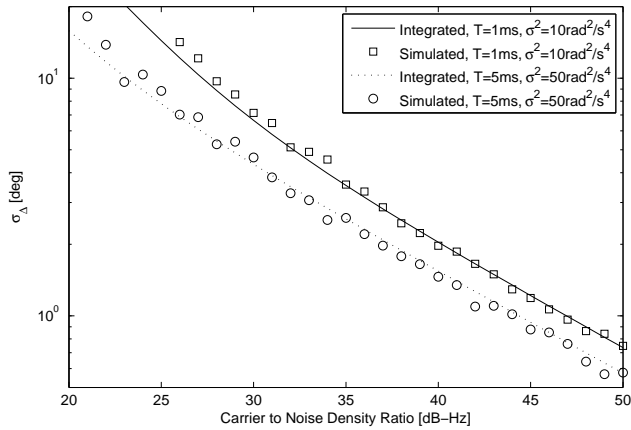


Fig. 2. Performance of IF-simulations compared to the evaluation of the variance-integral.

For a static receiver  $\mathbf{w}_{r,i} = \mathbf{0}$ ,  $\forall i$  and therefore the covariance of the random walk describing the receiver movements is set to zero. For a situation where the received measured carrier-phase is dominated by the receiver's oscillator, the performance of a multisatellite tracking loop is compared to a receiver using individual loops, see Fig. 3. In the high noise domain, the figure shows small offsets between the IF-simulated curves and the ones obtained by evaluating the integral of Equation 13. This is mainly due to the nonlinearity of the used arctangent discriminator.

The gain achieved by jointly tracking signals from ten satellites is found to range from 5 dB for low  $C/N_0$  up to  $> 8$  dB for high  $C/N_0$ , due to the spatial correlation between the signals from all satellites. By just using two satellites in the multisatellite loop, the gain achieved at low noise is approximately 3 dB. This leads to the conclusion that the gain observed for a multisatellite loop can be upper bounded by  $G_{K\text{Sat.}} \leq 10 \log_{10}(K)$ , where  $K$  is the number of satellites. This is in agreement with the

Cramér-Rao lower bound for an estimator, with different numbers of samples.

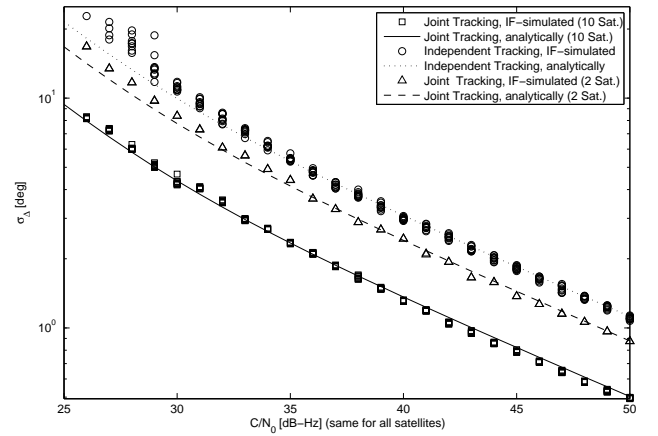


Fig. 3. Comparison of the performance of a multisatellite tracking loop (2 and 10 satellites) and traditional independent tracking loops.

Similarly the performance of a multifrequency loop can be evaluated, see Fig. 4. The gain for using the three Galileo frequencies jointly is in the order of 3 dB, which is in agreement with the rough upper bound found for the gain.

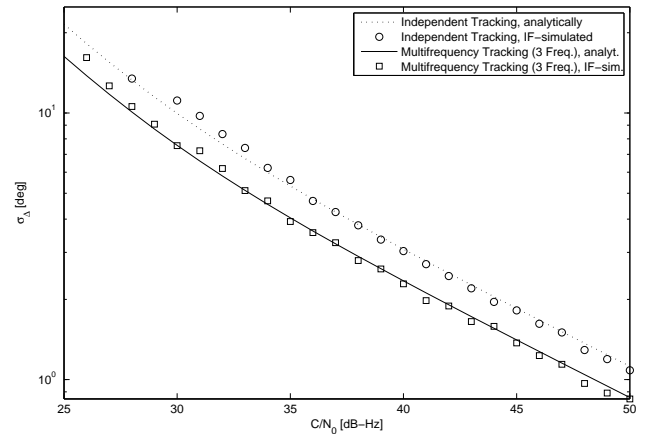


Fig. 4. Comparison of the performance of a multifrequency tracking loop (E1, E5a and E5b frequency) and traditional independent tracking loops.

To test the robustness of the joint tracking loop, a single-satellite attenuation scenario should be examined. At the beginning all of the ten satellites have a good signal strength ( $C/N_0 = 45$  dB-Hz). Later one satellite is heavily attenuated during an interval of four seconds (and also its entry in the measurement noise covariance matrix updated). The carrier-to-noise density ratio is shown in Figure 5. In Figure 6 the estimated phase for the attenuated satellite is plotted. As expected, when the noise is increased, the individual tracking loop starts to skip cycles (shown in the small box of the uppermost plot). Due to the perfect knowledge of the carrier-to-noise density ratio, the bandwidth of the loop is tightened and though the loop's carrier frequency doesn't drift away too much, such

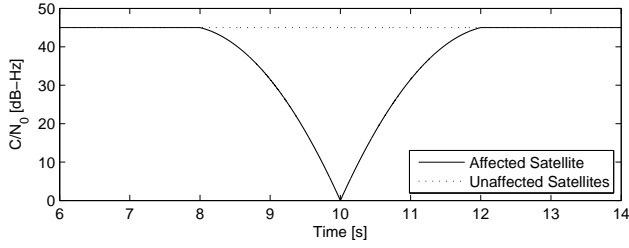


Fig. 5. The simulated carrier-to-noise density ratios for the scenario where one satellite is attenuated.

that after the recovery of the satellite a phase-lock can be achieved again.

The other two plots show the same scenario for a multisatellite tracking loop. For the bottom plot, the receiver was given full knowledge about the signal strengths on all satellites. Although the signal of one satellite was heavily attenuated phase lock could be maintained also during this period. One could argue now that it's unrealistic to have perfect  $C/N_0$ -knowledge. This case was simulated in the plot in the middle where the filter always assumed 45dB-Hz on all satellites.

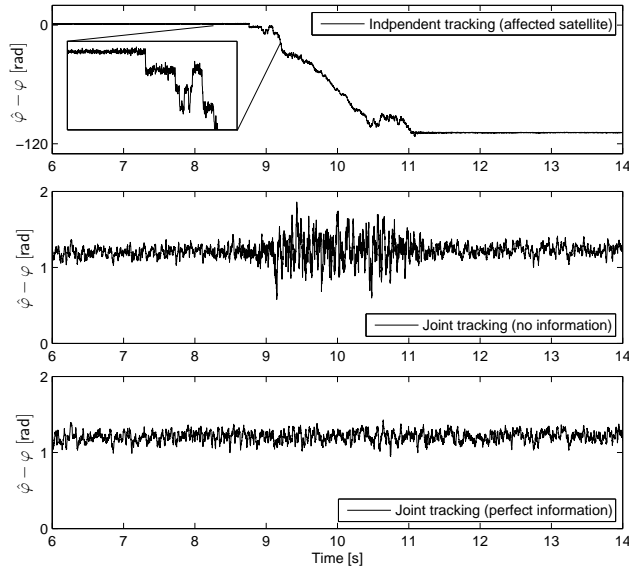


Fig. 6. Carrier-phase estimation (Integrated Doppler) for independent and multisatellite tracking.

The evaluation of the standard deviation of the carrier-phase error for the scenario with one attenuated satellite is evaluated in Figure 7. In the case of independent tracking loops, the performance of the unaffected satellites remains constant over all  $C/N_0$  values of the attenuated one. Also as known, the standard deviation of the affected satellite increases for a decreasing  $C/N_0$ . In the case of joint carrier-phase tracking, the weight of the attenuated satellite is adapted to its noise strength. Whenever the noise is very high, the satellite's tracking loop is dominated by measurements of the other satellites, meaning that its performance is mainly depending on the performance of the unaffected channels. In Figure 7 it can be seen that the carrier-phase error standard

deviation is always well below the often used margin of  $15^\circ$ . Therefore Cycle Slips won't occur even though the noise is dramatically increased.

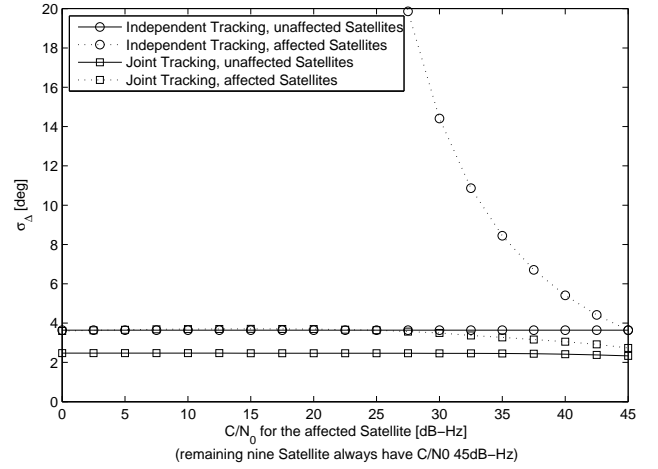


Fig. 7. Phase error standard deviation for the unaffected and attenuated satellites, compared for an independent and joint tracking receiver.

#### 4. PRN CODE TRACKING

So far the discussion was about carrier-phase tracking, mainly because this part is more critical in a GNSS receiver than the code-phase tracking. Nevertheless, in a situation where one satellite is masked for a short period, a receiver cannot benefit from joint tracking of multiple satellites if the code-phase was not stabilized as well during the outage. This motivates the extension of the approach described above to code- and carrier-phase tracking.

#### SYSTEM MODEL

The same derivations like presented for the carrier tracking can be used to find a model for the code tracking loop:

$$\underbrace{\begin{bmatrix} \Delta\tau_{m,i+1}^k \\ \Delta\dot{\tau}_{m,i+1}^k \\ \ddot{\tau}_{m,i+1}^k \\ \vdots \end{bmatrix}}_{\mathbf{x}_{\tau,i+1}} = \mathbf{A}_n \mathbf{x}_{\tau,i} + \mathbf{B}_0 \mathbf{u}_{\tau,m,i}^k + \mathbf{w}_{\tau,m,i+1}^k,$$

where  $\Delta\tau_{m,i}^k$  denotes the code-phase difference between the received  $m$ th signal (satellite  $k$ , frequency  $m$ ) and the locally generated replica,  $\Delta\dot{\tau}_{m,i}^k$  its time derivative. Here it's also assumed that a second-order NCO is used to generate the spreading code, i.e. phase and frequency can be steered. Therefore higher order derivatives of the received phase show up as absolute values as their corresponding component in the NCO is 0.

The basic model can be further split up into parts originating from the receiver and satellite movements, clocks and atmospheric effects. The basic difference to Equation 6 is a different scaling and a reversed sign for

the ionospheric delay:

$$\begin{aligned} \mathbf{x}_{\tau,m,i+1}^k &= \mathbf{A}_n \mathbf{x}_{\tau,m,i}^k + \frac{f_{\text{code},m}}{c} \left( (\mathbf{e}^k)^T \otimes \mathbf{I}_{n_r} \right. \\ &\quad \cdot (\mathbf{w}_{r,i+1} - \mathbf{w}_{r^k,i+1}) + \mathbf{w}_{\delta,i+1} + \mathbf{w}_{\delta^k,i+1} \\ &\quad \left. - \mathbf{w}_{I_m^k,i+1} + \mathbf{w}_{T^k,i+1} \right) + \mathbf{B}_0 \mathbf{u}_{\tau,m,i}^k. \end{aligned} \quad (14)$$

Stacking the two state vectors for the carrier- and the code-phase on each other, the final state vectors for each satellite and frequency can be found:

$$\underbrace{\begin{bmatrix} \mathbf{x}_{\varphi,m,i+1}^k \\ \mathbf{x}_{\tau,m,i+1}^k \end{bmatrix}}_{\mathbf{x}_{m,i+1}^k} = (\mathbf{I}_2 \otimes \mathbf{A}_n) \mathbf{x}_{m,i}^k + (\mathbf{I}_2 \otimes \mathbf{B}_0) \mathbf{u}_{m,i}^k + \mathbf{G}_m^k \mathbf{w}_{i+1}^k.$$

The measurement-equation (7) can easily be extended to include the code-phase measurements, e.g. together with the use of a normalized DLL discriminator [2].

## 5. CONCLUSION

In this paper a Multifrequency Multisatellite tracking loop was derived. The performance in terms of tracking error standard deviation was compared to the independent tracking. It was shown that the performance can substantially increased by jointly tracking the signals from multiple satellites and on multiple frequencies. As an example, during an outage of four second on one satellite, phase tracking was possible without leading to a Cycle Slip or loss of lock. An explanation was given by looking at the tracking error standard deviation for the system suffering from the outage. We therefore conclude that jointly tracking multiple signals significantly increases the robustness of a GNSS receiver.

\*

### References

- [1] J. W. Sennott and D. Senffner, "The use of satellite constellation geometry and a priori motion constraints for prevention of cycle slips in a GPS signal processor," *NAVIGATION, Journal of the Institute of Navigation*, vol. 39, no. 2, pp. 217 – 236, 1992.
- [2] B. W. Parkinson and J. J. S. Jr., *Global Positioning System: Theory and Applications*. Progress in Astronautics and Aeronautics, 1996, vol. Volume I.
- [3] T. Pany, R. Kaniuth, and B. Eissfeller, "Deep integration of navigation solution and signal processing," in *Proceedings of the ION GNSS 18th International Technical Meeting of the Satellite Division*, Long Beach, CA, September 2005.
- [4] P. Henkel, K. Giger, and C. Gunther, "Multifrequency, multisatellite vector phase-locked loop for robust carrier tracking," *Selected Topics in Signal Processing, IEEE Journal of*, vol. 3, no. 4, pp. 674–681, Aug. 2009.
- [5] D. Polk and S. Gupta, "Quasi-optimum digital phase-locked loops," *IEEE Transactions on Communications*, vol. 21, no. 1, pp. 75–82, Jan 1973.
- [6] W. Hurd, J. Statman, and V. Vilnrotter, "High dynamic GPS receiver using maximum likelihood estimation and frequency tracking," *IEEE Transactions on Aerospace and Electronic Systems*, vol. AES-23, no. 4, pp. 425–437, July 1987.
- [7] M. L. Psiaki and H. Jung, "Extended Kalman filter methods for tracking weak GPS signals," in *Proceedings of the 15th International Technical Meeting of the Satellite Division of the Institute of Navigation ION GPS 2002*, Oregon, September 2002, pp. 2539–2553.

- [8] A. Patapoutian, "On phase-locked loops and Kalman filters," *IEEE Transactions on Communications*, vol. Volume 47, no. 5, pp. 670–672, May 1999.
- [9] G.-I. Jee, "GNSS receiver tracking loop optimization for combined phase, frequency and delay locked loops," in *Proceedings of the European Navigation Conference ENC – GNSS 2005*, Munich, July 2005.
- [10] E. D. Kaplan and C. J. Hegarty, Eds., *Understanding GPS – Principles and Applications*, 2nd ed. Artech House, 2006.
- [11] R. G. Brown and P. Y. C. Hwang, *Introduction to Random Signals and Applied Kalman Filtering*. John Wiley & Sons, Inc., 1992.
- [12] C. O'Driscoll and G. Lachapelle, "Comparison of traditional and Kalman filter based tracking architectures," in *Proceedings of the European Navigation Conference ENC – GNSS 2009*, Naples, May 2009.
- [13] V. A. Vilnrotter, S. Hinedi, and R. Kumar, "Frequency estimation techniques for high dynamic trajectories," *IEEE Transactions on Aerospace and Electronic Systems*, vol. Volume 25, no. 4, July 1989.
- [14] K. Giger, P. Henkel, and C. Günther, "Joint satellite code and carrier tracking," in *ION International Technical Meeting*, San Diego, January 2010, to appear.
- [15] A. V. Oppenheim and R. W. Schaffer, *Discrete-Time Signal Processing*. Englewood Cliffs, NJ: Prentice-Hall, Inc., 1989.
- [16] W. C. Lindsey, *Synchronization Systems in Communication and Control*. Englewood Cliffs, NJ: Prentice-Hall, Inc., 1972.